OPTRONIC™
LABORATORIES

HYPERSPECTRAL MICROSCOPE IMAGING METHODS TO CLASSIFY GRAM-POSITIVE AND GRAM-NEGATIVE FOODBORNE PATHOGENIC BACTERIA

B. Park, Y. Seo, S. C. Yoon, A. Hinton Jr.,
W. R. Windham, K. C. Lawrence

June 2015

Reprint Number: R48 | Cover Sheet Updated: Apr 2019 | OptronicLabs.com

HYPERSPECTRAL MICROSCOPE IMAGING METHODS TO CLASSIFY GRAM-POSITIVE AND GRAM-NEGATIVE FOODBORNE PATHOGENIC BACTERIA

B. Park, Y. Seo, S. C. Yoon, A. Hinton Jr., W. R. Windham, K. C. Lawrence

ABSTRACT. *An acousto-optic tunable filter (AOTF)-based hyperspectral microscope imaging (HMI) method has potential for rapid identification of foodborne pathogenic bacteria from micro-colonies with a cell level. In this study, we successfully developed a method to acquire quality hyperspectral microscopic images from various gram-negative and gram-positive bacteria live cells. Among the contiguous spectral images from the visible/NIR region between 450 and 800 nm, the scattering intensity of spectral images was distinct at mostly visible wavelengths. Specifically, the scattering peak intensity was distinct at 458, 498, 522, 546, 574, 590, 646, 670, and 690 nm for* Staphylococcus*. Similarly, distinct peak spectra were observed at 462, 498, 522, 546, 574, 598, 642, 670, and 690 nm for* Salmonella*. For both cases, the scattering intensity of outer cell membranes was brighter than that of inner membranes except at 546 nm, which was possibly caused by excitation of the metal-halide lighting source. The scattering intensity from a single cell varied with the wavelength as well as the type of bacteria. The overall variability of intensity was 31.2% for gram-negative (*Salmonella*) and 42.7% for gram-positive (*Staphylococcus*) bacteria. With scattering intensity data from five serotypes of* Salmonella *(Kentucky, Enteritidis, Typhimurium, Infantis, and Heidelberg) and five species of* Staphylococcus *(*aureus*,* haemolyticus*,* hyicus*,* simulans*, and* sciuri*) bacterial cells, a classification accuracy of 99.9% with a kappa coefficient of 0.9998 was obtained from the support vector machine (SVM) classification algorithm.*

Keywords*. Acousto-optic tunable filter, Bacteria detection, Foodborne pathogen, Hyperspectral, Microscopy,* Salmonella*, Serotype,* Staphylococcus*.*

Food safety is a worldwide issue for public health. Each year, one in six Americans gets sick from foodborne diseases. The challenges in terms of food safety continue to arise in unpredictable ways due to changes in food production and supply; changes in the environment causing food contamination; rising numbers of multi-state outbreaks; new and emerging germs, toxins, and antibiotic resistance; and new and different contaminated foods, such as prepackaged raw materials. During the past decade, about 3,562 outbreaks in single food commodities, including poultry, eggs, beef, pork, leafy greens, fruits, nuts, and dairy, caused illness (CDC, 2012). The germs and related foods responsible for most foodborne illnesses were *Salmonella* in eggs, poultry, meat, and produce; *Campylobacter* in poultry; *E. coli* O157 in ground beef, leafy greens, and raw milk; *Listeria* in produce and deli meats; *Vibrio* in raw oysters; *Norovirus* in sandwiches and salads; and *Toxoplasma* in meats. In 2011, about 48 million incidences of foodborne illness occurred, resulting in 128,000 hospitalizations and 3,000 deaths in the U.S. The estimated cost of foodborne illness in the U.S. is approximately $77.7 billion per year (Scharff, 2012). Among serious outbreaks, *Salmonella* (15.1%) had the most infections and incidence cases, followed by *Campylobacter* (13%) (CDC, 2011). Every year, *Salmonella* is estimated to cause one million illnesses in the U.S., with 19,000 hospitalizations and 380 deaths. An outbreak of *Staphylococcal* food poisoning from a military lunch sickened 13 people in 2012 (MMWR, 2013).

Current detection methods for foodborne pathogens include ISO method 6579 (ISO, 2002), direct fluorescence antibody detection (Munson et al., 1976), immunodetection such as enzyme-linked immunosorbant assay (ELISA) (Tian et al., 1996), and polymerase chain reaction (PCR) (Correa et al., 2006). However, all these methods are limited for practical use due to time-consuming processes, cumbersome results, and sensitivity concerns. Among many other detection methods, traditional culture-based methods remain the most reliable and accurate "gold standard" techniques for pathogen detection (Velusamy et al., 2010). These methods involve culturing an inoculum to amplify the microbial cell numbers, followed by plating on

Submitted for review in July 2014 as manuscript number IET 10832; approved for publication by the Information, Technology, Sensors, & Control Systems Community of ASABE in December 2014.

Mention of trade names or commercial products in this article is solely for the purpose of providing specific information and does not imply recommendation or endorsement by the USDA. The USDA is an equal opportunity provide and employer.

The authors are **Bosoon Park, ASABE Member,** Research Agricultural Engineer, **Youngwook Seo,** Postdoctoral Research Associate, **Seung-Chul Yoon, ASABE Member,** Research Electronic Engineer, **Arthur Hinton Jr.,** Research Microbiologist, **William R. Windham,** Research Animal Physiologist, and **Kurt C. Lawrence, ASABE Member,** Research Leader, USDA-ARS Russell Research Center, Athens, Georgia. **Corresponding author:** Bosoon Park, Russell Research Center, P.O. Box 5677, 950 College Station Road, Athens, GA, 30604-5677; phone: 706-546-3396; e-mail: bosoon.park@ars.usda.gov.

a selective or differential medium to generate colonies that can be detected based on their distinctive color as well as morphology. Culture-based methods are inexpensive and very sensitive with good specificity. They also can provide both colony count estimations and qualitative information on the microorganisms present in food samples. However, culture-based methods are labor intensive, and at least two or three days are needed for the microorganisms to multiply to visible colonies for a presumptive positive result. Another challenge is that unwanted background microflora grow together with the target microorganisms on agar media and often look similar. Hence, highly skilled technicians are needed to identify presumptive positive colonies by trial and error. However, this limitation could be improved with optical detection methods. Therefore, a more sensitive, accurate, and rapid pathogen detection method is needed for practical use with better performance.

Hyperspectral imaging is a candidate to meet the above requirement for real-time, *in situ* foodborne pathogen detection with less colony biomass by minimizing incubation time (Park et al., 2012a). Hyperspectral imaging was developed as a powerful technique in terrestrial remote sensing, and this technique continues to be utilized in medical, biological, agricultural, and industrial applications. Hyperspectral imaging combines aspects of conventional imaging with spectrophotometry and radiometry. This technique is capable of providing an absolute radiometric measurement over a contiguous spectral range for every pixel of an image. Thus, the data from a hyperspectral image contain two-dimensional spatial information as well as spectral information. These data can be considered a three-dimensional "hypercube" that can provide physical and/or chemical information on the material under test. This information includes physical and geometric observations of size, orientation, shape, color, and texture, in addition to chemical and molecular information such as water, fat, proteins, and other hydrogen-bonded constituents.

Several different hyperspectral imaging platforms exist, including pushbroom, acouto-optic tunable filter (AOTF), filter wheel, and liquid crystal tunable filter (LCTF). When selecting a platform, the user needs to consider several parameters, including imaging technique, spectral and spatial resolution, data capture, transmission intensity, and switching speed. Pushbroom-based platforms use dispersive and mechanical scanning with a grating-prism-grating method. The pushbroom technique has high spectral resolution, relatively high transmission, and variable switching speed. In contrast, AOTF uses a solid-state non-linear crystal to generate hyperspectral images. It has dynamically variable spectral resolution and variable sequential band-pass with random access ability. An LCTF-based platform (Wang et al., 2012) has fixed and defined *a priori* spectral resolution and fixed sequential band-pass with random-access image capture. This platform has relatively lower transmission ability. Similar to AOTF, the switching speed is not fast. Thus, the selection of a hyperspectral imaging platform is fully dependent on the application. Two platforms, including pushbroom (Windham et al., 2012; Yoon et al., 2013) and AOTF (Park et al., 2012a), were developed for the detection of contaminants and foodborne pathogens. The researchers demonstrated these two hyperspectral imaging systems, using pushbroom for bacterial colonies on agar plates (Windham et al., 2012; Yoon et al., 2013) and AOTF for microscopic imaging of live bacterial cells from microcolonies on agar plates (Park et al., 2012a).

Based on current methods from the USDA Food Safety and Inspection Service (USDA-FSIS, 2014), at least four days are required to detect and identify non-O157 Shiga toxin-producing *E. coli* (STEC). Because rapidly and accurately identifying STEC colonies by naked eye is challenging due to the phenotypic variability in STEC populations and the presence of background microflora for foodborne outbreaks, new objective and accurate methods are needed to reduce the time required to identify presumptive positive STEC colonies on agar plates. Our research group previously developed a macro-scale hyperspectral imaging technique to identify STEC serogroups by acquiring both spatial and spectral information from every pixel for each STEC serogroup on Rainbow agar plates (Windham et al., 2012; Yoon et al., 2013). The spectral fingerprints of the bacteria provided by the hyperspectral imaging system can be used for detection and identification of pathogens grown on agar media. In particular, a VNIR hyperspectral imaging technique with multivariate classification models was developed to differentiate colonies of non-O157 STEC bacteria as well as *Campylobacter* (Yoon et al., 2009). Thus, hyperspectral imaging has potential for rapidly identifying colonies of non-O157 STEC serogroups on Rainbow agar plates inoculated with mixed cultures. Spatial and spectral data analysis demonstrated that the differences in appearance of the non-O157 STEC serogroup colonies were mainly due to differences in the absorption bands and color tones. The color was the major feature exploited in the classification model for STEC detection, with 97% classification accuracy (Yoon et al., 2013). However, this macro-scale hyperspectral imaging method requires an incubation process for fully grown bacterial colonies on agar plates for measurement.

The objective of the research reported in this article is to develop a new micro-scale optical method to identify foodborne pathogens with AOTF-based hyperspectral microscope imaging (HMI) technology. More specifically, classification models to identify gram-positive and gram-negative foodborne pathogenic bacteria were developed for rapid detection of foodborne pathogens.

MATERIALS AND METHODS

PREPARATION OF BACTERIAL CULTURES

Five gram-negative *Salmonella* serotypes (Kentucky, Enteritidis, Typhimurium, Infantis, and Heidelberg) and five species of gram-positive *Staphylococcus* (*aureus*, *haemolyticus*, *hyicus*, *simulans*, and *sciuri*) were obtained from the USDA-ARS Poultry Processing and Swine Physiology Research Unit in Athens, Georgia. Bacterial cultures were prepared by inoculating pure isolates into trypticase soy broth (TSB) tubes and incubated at 35°C ±2°C for 18 to 24 h. The overnight-grown cultures of all five species of *Staphylococcus* were centrifuged at 5000 rpm for 10 min.

The bacterial pellet was resuspended in deionized (DI) water. From the overnight-grown cultures of five serogroups of *Salmonella*, 10-fold serial dilutions were prepared in 0.1% peptone water, and 10^{-6} final dilutions were plated onto brilliant green sulfa (BGS) agar plates in duplicate. All plates were incubated at 35°C ±2°C for 24 h. One colony was picked from the BGS plate of each *Salmonella* serotype and resuspended in 10 µL of DI water. For hyperspectral microscope imaging, 3 µL of the bacterial suspensions of all *Salmonella* serotypes and *Staphylococcus* species were spread in the center of a microscopic glass slide, in an approximately 20 mm × 20 mm area, followed by drying for 10 min in a biosafety cabinet. After drying, an additional 0.8 µL of DI water was added in the center of the slide, and a cover slip was placed on top of the sample.

Hyperspectral Microscope Imaging System

The HMI system (fig. 1) consists of an upright microscope (Eclipse e80i, Nikon, Lewisville, Tex.), acousto-optic tunable filters (AOTF) (HSi-400, Gooch & Housego, Orlando, Fla.), a high-performance cooled electron-multiplying charge-coupled device (EMCCD) 16-bit camera (iXon, Andor Technology, Belfast, Northern Ireland), and a darkfield illumination source (CytoViva 150 unit, 24 W metal-halide, CytoViva, Auburn, Ala.). The AOTF used for this research has a high-speed, high-throughput, random-access solid-state optical filter with an adjustable optical pass-band and exceptionally high rejected light levels. The AOTF delivers diffraction-limited image quality with variable bandwidth resolution down to within 2 nm in the spectral range from 450 to 800 nm. The AOTF-based HMI system is a scanning spectrophotometer employing an instrument technology with no moving parts, capable of high scan speeds, and providing random access to any number of wavelengths selected prior to scanning.

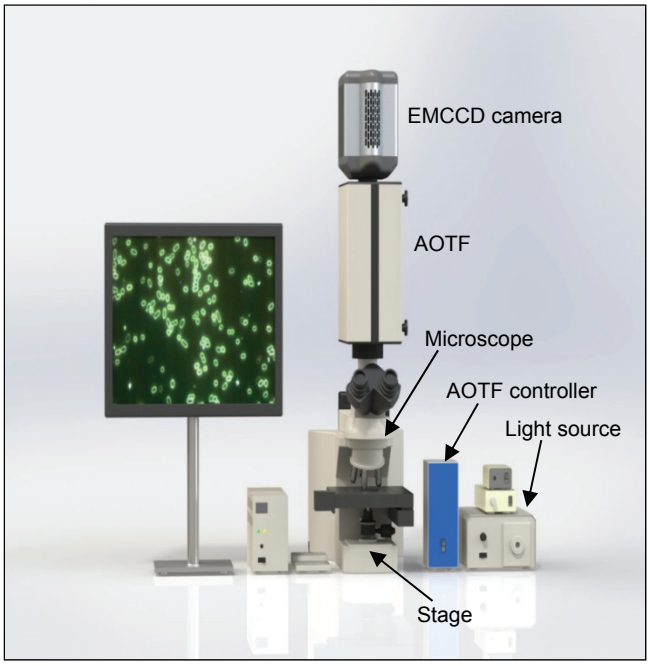

Figure 1. AOTF hyperspectral microscope imaging system.

Darkfield Illumination

Because darkfield microscopy is an effective technique for live and unstained biological samples, such as foodborne cellular organisms, we used darkfield illumination as the lighting technique in this study. Darkfield illumination enhances the contrast in unstained bacterial samples. This technique produces a dark background with bright objects, which can show bacterial cells distinctly. In contrast to brightfield illumination, which measures the absorbance of target objects, darkfield illumination enables us to measure the scattered intensity from target objects, i.e., bacterial cells in this case. For our experiment with the upright microscope, light enters the microscope to illuminate the bacterial cells. A specially designed disk blocks some of the light from the light source (metal-halide in our experiment), and the light leaves an outer ring of illumination. The condenser lens focuses the light toward the cells so that the light enters the cells. Most of the light energy is directly transmitted, while some is scattered from the cell. The scattered light enters the objective lens, while the directly transmitted light that misses the lens is not collected due to a direct illumination block. Thus, only the scattered light produces the image, while the directly transmitted light is omitted. The main limitation of this technique is the low light intensity, which means that the sample must be very strongly illuminated to produce a quality image. Therefore, we used a metal-halide light source.

Bacterial Cell Immobilization

Because hyperspectral image acquisition at wavelengths from 450 to 800 nm in 4 nm increments requires a longer imaging time than regular microscope imaging, the challenge of the HMI method was to immobilize the live cells completely during image acquisition; otherwise, the hyperspectral data or hypercube would not represent the spectral characteristics of live bacterial cells. Thus, immobilization of the live bacterial cells is the most crucial aspect in acquiring high-quality images. Based on several protocols tested, we used a modified drying method (Park et al., 2012b) to immobilize live cells for quality image acquisition. With this method, three types of cell movement, including bacterial cell motility and bacteria movement with the flow of the liquid media, were not observed. Although some Brownian motion (Park et al., 2012b) was observed, most bacterial cells were thoroughly immobilized during the scan. Thus, images were successfully acquired with the HMI system from live bacterial cells without any bacterial mobility.

Gram-Negative and Gram-Positive Bacteria

Bacteria are traditionally divided into two main groups, gram-negative and gram-positive, based on their gram-stain retention. This classification system is ambiguous, as it can refer to three distinct aspects, including staining result, cell-envelope organization, and taxonomic group. Compared to gram-positive bacteria, gram-negative bacteria are more resistant to antibodies because of their impenetrable cell wall, which is due to an additional outer membrane. In this study, *Salmonella* and *Staphylococcus* were selected as gram-negative and gram-positive samples, respectively. Figure 2 shows hyperspectral microscopic composite im-

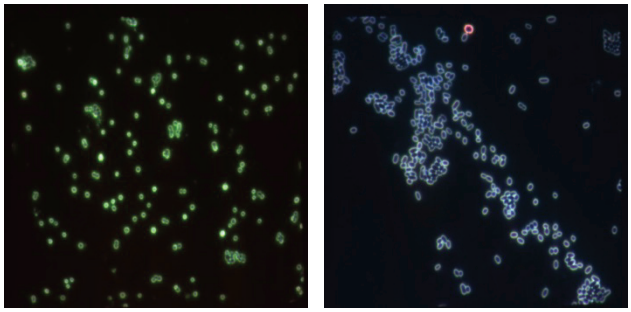

(a) (b)

Figure 2. Hyperspectral composite images of (a) gram-positive bacteria (*Staphylococcus aureus*) and (b) gram-negative bacteria (*Salmonella* Enteritidis).

ages based on the wavelengths 648 nm (red), 550 nm (green), and 436 nm (blue) of *Staphylococcus aureus* (fig. 2a) and *Salmonella* Enteritidis (fig. 2b). These images show different morphologies, with round shapes for the gram-positive bacterial cells and elliptical shapes for the gram-negative bacterial cells.

Hyperspectral Microscope Image Acquisition

Figure 3 shows the procedure for hyperspectral microscope image acquisition and analysis of live bacterial cells. Foodborne bacteria (gram-negative *Salmonella* and gram-positive *Staphylococcus*) isolated from poultry carcass rinses were used for the image data. Images of five *Salmonella* serotypes (Enteritidis, Typhimurium, Heidelberg, Kentucky, and Infantis) and five *Staphylococcus* species (*aureus*, *haemolyticus*, *hyicus*, *sciuri*, and *simulans*) were acquired with the AOTF-based HMI system. In this experiment, visible/NIR hyperspectral microscope images were collected in TIFF format at wavelengths from 450 to 800 nm with 2 nm bandwidth, 4 nm spectral intervals, individual scanning exposure time of 250 ms, and a gain of 9, as selected in a previous study (Park et al., 2012a; Park et al., 2012b) for quality image acquisition. All images were acquired with darkfield illumination using a metal-halide lighting source and a spectral sweep mode for collecting contiguous spectral images (Park et al., 2012b). The acquired images (in TIFF format) were converted to hyperspectral image format with HSiAnalysis software (Gooch & Housego, Orlando, Fla.).

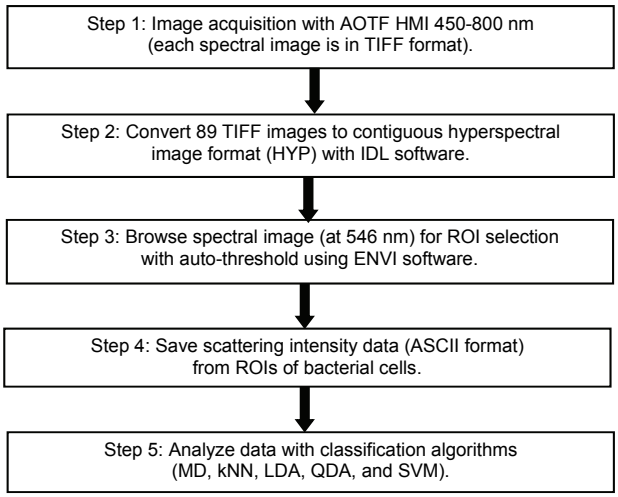

Figure 3. Flowchart of procedure for hyperspectral microscope image acquisition and analysis of live bacterial cells.

Hyperspectral Microscope Image Analysis

After image conversion was completed, one spectral image of 546 nm (fig. 4d) was selected to create a region of interest (ROI) from the bacterial cells with ENVI software (version 4.8, Exelis Visual Information Solutions, Inc., Boulder, Colo.). The scattering intensity data from the ROI of each cell were saved for further analysis. R software (version 3.0.1, R Project for Statistical Computing, Vienna, Austria) was used for developing classification methods with five different algorithms, including Mahalanobis distance (MD), *k*-nearest neighbor (kNN), linear discriminant analysis (LDA), quadratic discriminant analysis (QDA), and support vector machine (SVM), to identify the different species and serotypes using their spectral signatures collected with the HMI system.

Classification Methods

Mahalanobis Distance

Mahalanobis distance (MD) (De Maesschalck et al., 2000) is the most commonly used distance measure for multivariate chemometrical techniques in the principal component (PC) space. MD is used for several different purposes, such as detection of outliers, selection of calibration samples from a large set of measurements, and obser-

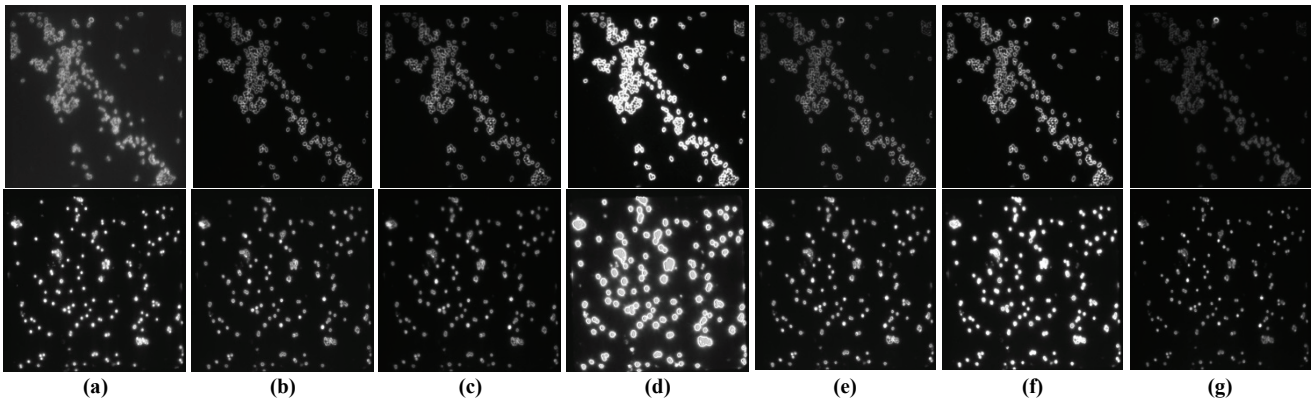

(a) (b) (c) (d) (e) (f) (g)

Figure 4. Image comparison of *Salmonella* Enteritidis (top row) and *Staphylococcus aureus* (bottom row) at wavelengths of (a) 458 nm, (b) 498 nm, (c) 522 nm, (d) 546 nm, (e) 574 nm, (f) 590 nm, and (g) 670 nm.

vation of differences between two data sets. In pattern recognition, MD is applied in clustering techniques such as *k*-nearest neighbor (kNN) (Vandeginste et al., 1998) and in discrimination techniques such as linear and quadratic analysis (LDA and QDA) (Wu et al., 1996). MD measures the distance using the variance-covariance of two points, as shown in equation 1.

$$\mathrm{MD}_i = \sqrt{(x_i - \bar{x})\, C_x^{-1}\, (x_i - \bar{x})^T} \quad (1)$$

where C_x is the variance-covariance matrix of two variables, x_1 and x_2. The ellipse represents the equal MDs toward the center point of the sample data. In order to discriminate two classes, a criterion is necessary. Using prior knowledge, a threshold value is determined.

k-Nearest Neighbor

The *k*-nearest neighbor (kNN) method (Vandeginste et al., 1998) is one of the simplest methods for pattern classification. It is a non-parametric method for classifying objects based on the closest training examples in the feature space. For high-dimensional datasets (i.e., more than ten dimensions), dimension reduction is usually performed prior to applying the kNN algorithm. The kNN method classifies a given unlabeled example based on its closeness to the k closest labeled examples in the training data set. Integer k is the number of examples used to measure the distance from unknown example x_u. The kNN method uses the Euclidean distance from x_u to the closest examples.

Linear Discriminant Analysis

Linear discriminant analysis (LDA) (Wu et al., 1996; Dixon and Brereton, 2009) is a method for finding a linear combination of features that separates two or more classes of objects. Similar to principal component analysis (PCA) and factor analysis, LDA looks for linear combinations of variables that best explain the data, so LDA explicitly attempts to model the difference between the classes of data. LDA seeks to reduce the dimensionality of the data matrix while preserving as much of the class-discriminating information as possible.

$$y = w^T x \quad (2)$$

where w is the projection vector. In order to find a good projection vector (i.e., to find the maximum distance between two classes), LDA utilizes the Mahalanobis distance (Park et al., 2007). However, LDA fails if the discriminating information is in the variance of the data. Furthermore, if the distributions are significantly non-Gaussian, then LDA is limited in classifying data with complex structures.

Quadratic Discriminant Analysis

Quadratic discriminant analysis (QDA) is a more general version of the linear classifier, so it is used in statistical classification to separate two or more classes of objects by a quadric surface. Similar to LDA, QDA assumes that the measurements from each class are normally distributed. However, unlike LDA, there is no assumption in QDA that the covariance of each class is identical. Similar to LDA, QDA uses the Mahalanobis distance to measure the discriminating information between two classes (Dixon and Brereton, 2009). In contrast, even if the distributions are significantly non-Gaussian in the hyperbolic space, the QDA projections may preserve the complex structures in the data needed for classification.

Support Vector Machine

Support vector machine (SVM) (Furey et al., 2000) is a supervising learning algorithm with associated learning algorithms that analyze data and recognize patterns used for classification. SVM can efficiently perform non-linear classification in a high-dimensional feature space. SVM constructs a hyperplane in a high-dimensional space, which can be used for classification. Intuitively, good separation is achieved by the hyperplane that has the largest distance to the nearest training data point of any class. SVM solves binary classification problems by creating an optimal hyperplane that maximizes the distance between the boundary points of two classes. It can be used to solve both linear and non-linear problems. The hyperplane is defined as follows:

$$f(x) = x^T w + b_0 = 0 \quad (3)$$

where x is the training data set, w is normal to the hyperplane, $x^T w$ is the inner product between x and w, and b_0 is the minimum distance from the origin to the hyperplane; $1/\|w\|$ is the perpendicular distance from the hyperplane to the boundary of each class.

To evaluate the developed classification models, cross-validation was conducted using a 10-fold cross-validation method. The total data set from the ROIs was approximately 703,000 pixels. To prepare the data for cross-validation, the whole data set was divided into 30 equal parts. In each iteration of the cross-validation, a part of the data (30% of the whole data set, N = 23,000 pixels) was selected arbitrarily. The remaining data (70% of the whole data set, N = 680,000 pixels) were used as the validation data set. This cross-validation process was iterated ten times.

RESULTS AND DISCUSSION

From a total of 89 spectral images from each bacterial sample acquired by the HMI system, figure 4 shows spectral images acquired with 250 ms integration time and a gain of 9 from gram-negative *Salmonella* Enteritidis and gram-positive *Staphylococcus aureus* at wavelengths of 458, 498, 522, 546, 574, 590, and 670 nm. As mentioned earlier, because the scattering intensity of the spectral images was higher at 546 nm than at other wavelengths, we used this image as a template for the ROI to generate image data for classification.

CHARACTERISTICS OF HYPERSPECTRAL IMAGES OF GRAM-NEGATIVE AND GRAM-POSITIVE BACTERIA

Among five different serotypes or species of both gram-negative and gram-positive bacteria, *Salmonella* Enteritidis and *Staphylococcus aureus* were selected to demonstrate hyperspectral microscopic images and the corresponding spectral characteristics based on cell structure or morphology.

Hyperspectral Image of Salmonella *Enteritidis*

Figure 5 shows a hyperspectral microscope image of *Salmonella* Enteritidis with a region of interest (ROI). To compare the spectral signatures of the inner and outer membranes of the cell, two scattered ROIs, one from the inner membrane (green) and the other from outer membrane (red), were captured separately from *Salmonella* Enteritidis bacterial cells. Figure 6 compares the spectral signatures of the inner (4,956 pixels) and outer (12,846 pixels) membranes of *Salmonella* Enteritidis bacterial cells. The scattering intensity of the outer membrane was higher than that of the inner membrane at wavelengths of 498, 522, 546, 574, and 598 nm. However, the scattering intensity of the outer membrane was lower than that of the inner membrane at 462, 670, and 690 nm, which means that possibly less scattering occurred in the outer membrane of the gram-negative cells. As seen in figure 6, the intensities of the two membranes were similar at 474, 626, and beyond 742 nm. However, the intensity distribution and spectral patterns could be changed slightly if other parameters are changed, such as the integration time and gain (Park et al., 2012a). Therefore, a protocol to calibrate the HMI system is needed to ensure the robustness of this micro-scale optical detection method.

Spectral Signature of Salmonella *Enteritidis*

Figure 7 shows the mean spectra and standard deviation (SD) of scattering intensity from *Salmonella* Enteritidis. As seen in figures 7a and 7b, the spectral patterns from the inner and outer cell membranes were similar, and both had peaks at wavelength of 462, 498, 522, 546, 574, 598, 642, 670, and 690 nm. However, the SD of each spectrum varied with the wavelength.

Table 1 summarizes the mean and SD values of scattering intensity and the percent variation with corresponding wavelengths for *Salmonella* bacterial cells. Based on the spectral data for *Salmonella* Enteritidis, less spectral variation (27.6%) was observed for the inner membrane than for the outer membrane (30.6%). In addition, the spectral variation of the inner and outer membranes was much less in the NIR range (21% inner and 22% outer at 722 nm) than

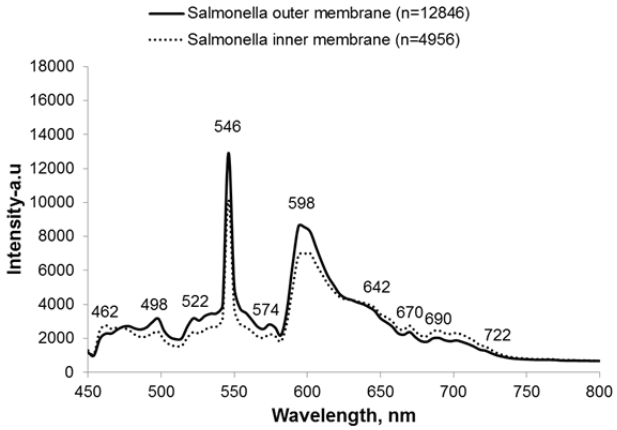

Figure 6. Comparison of spectral signatures from inner and outer membranes of gram-negative (*Salmonella* Enteritidis) bacterial cells.

in the visible range. The highest variation (34%) of the inner membrane was observed at 598 nm, followed by 33% at 546 nm. However, the highest variation (36%) of the outer membrane was observed at 598 nm, followed by 34% at 642 nm. The range of spectral variation was between 24% and 29% for the inner membrane, while the range of spectral variation for the outer membrane was higher (between 27% and 32%). This higher scattering variability for the outer cell membrane could be caused by the additional membrane of gram-negative bacteria.

Hyperspectral Image of Staphylococcus aureus

Figure 8 shows a hyperspectral microscope image of *Staphylococcus aureus* with a region of interest (ROI). In contrast with the gram-negative bacteria, the gram-positive bacteria have round shapes. Similar to *Salmonella*, two ROIs for the inner (green) and outer (red) membranes were acquired from *Staphylococcus aureus* bacterial cells to compare the spectral signatures of the inner and outer membranes of the gram-positive bacteria.

Figure 9 shows the spectral signatures of the inner (3,611 pixels) and outer (11,901 pixels) membranes of *Staphylococcus aureus* bacterial cells. The peaks of scatter-

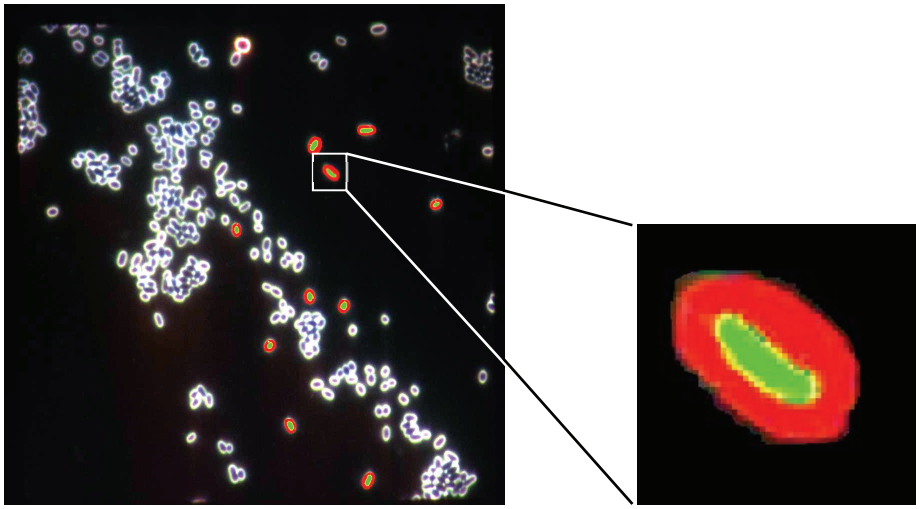

Figure 5. Hyperspectral microscope image of gram-negative (*Salmonella* Enteritidis) bacterial cells with a region of interest (ROI) showing the inner membrane (green) and outer membrane (red).

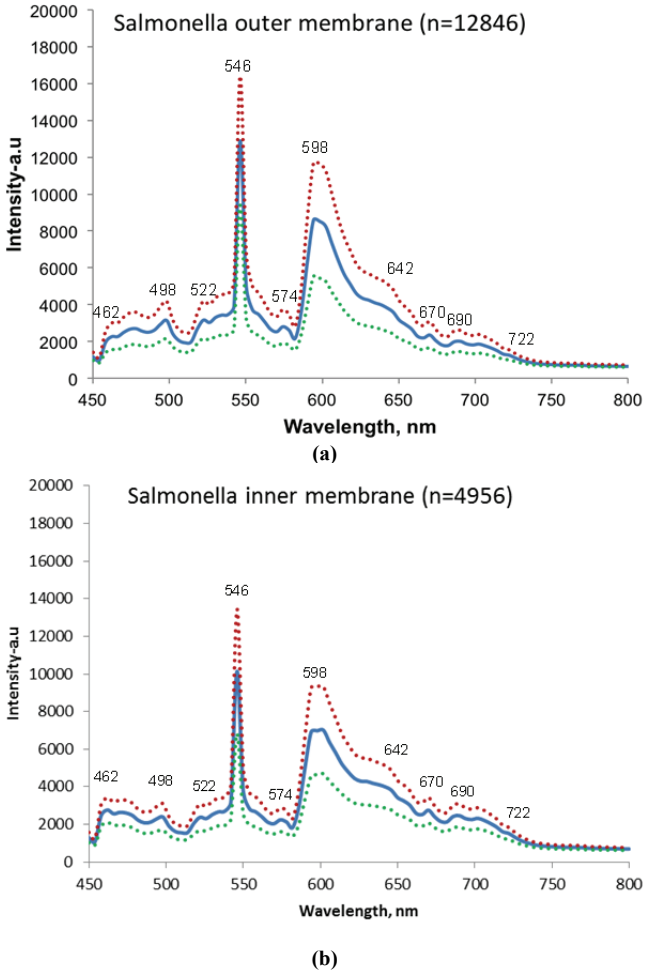

Figure 7. Mean and standard deviation of spectra from (a) outer and (b) inner membranes of gram-negative (*Salmonella* Enteritidis) bacterial cells (solid line is mean scattering intensity, and dotted lines are standard deviation of intensity at observed spectral bands).

ing intensity were higher for the outer membrane than for the inner membrane at 498, 522, 574, and 590 nm. However, the scattering intensity of the outer membrane was lower than that of the inner membrane at 458, 642, 670, and 690 nm, which suggests that possibly less scattering occurred in the outer membranes of the gram-positive bacteria. For *Staphylococcus aureus*, the scattering intensities of the two membranes were similar at 478, 622, and beyond 742 nm. However, similar to the gram-negative bacteria, the spectral patterns could be changed if different values of integration time and gain were used for the imaging system (Park et al. 2012a). Thus, a calibration protocol for the HMI system needs to be developed for optical detection of foodborne bacteria.

Table 1. Mean and standard deviation with corresponding wavelength of scattering intensity from *Salmonella* Enteritidis as measured by the hyperspectral microscope imaging system.

Salmonella Enteritidis	Wavelength (nm)	Mean	SD	Variation (%)
Inner membrane (n = 4,956)	462	2769	655	24
	498	2396	704	29
	522	2380	700	29
	546	10140	3309	33
	574	2245	628	28
	598	6982	2351	34
	642	4000	1125	28
	670	2754	679	25
	690	2471	615	25
	722	1523	322	21
	Average variation = 27.6%			
Outer membrane (n = 12,846)	462	2286	727	32
	498	3168	1025	32
	522	3186	1017	32
	546	12912	3510	27
	574	2829	919	32
	598	8550	3108	36
	642	3851	1300	34
	670	2377	715	30
	690	2036	584	29
	722	1279	276	22
	Average variation = 30.6%			

Spectral Signature of Staphylococcus aureus

Figure 10 shows the mean spectra and standard deviation (SD) of scattering intensity from *Staphylococcus aureus*. As seen in figures 10a and 10b, the spectral patterns from the inner and outer cell membranes were similar. Spectral peaks for both membranes were observed at wavelengths of 458, 498, 522, 546, 574, 590, 646, 670, and

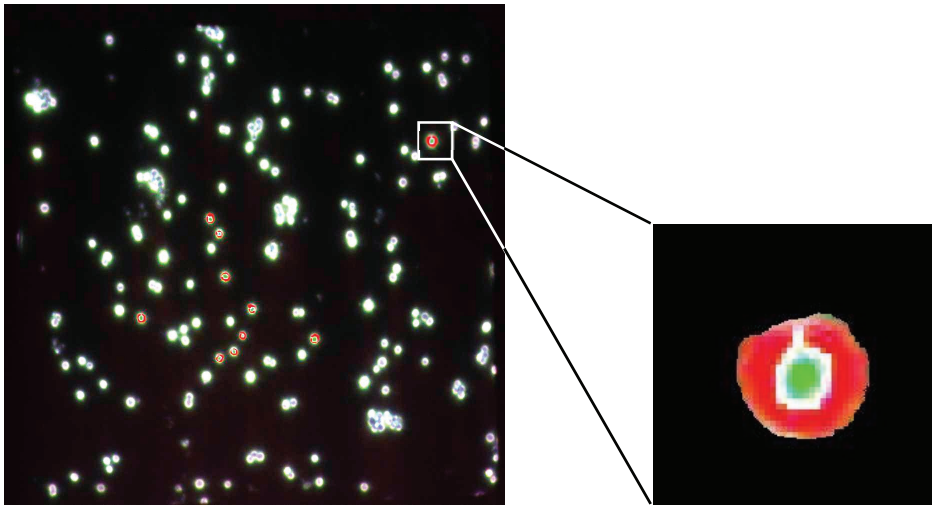

Figure 8. Hyperspectral microscope image of gram-positive (*Staphylococcus aureus*) bacterial cells with a region of interest (ROI) showing the inner membrane (green) and outer membrane (red).

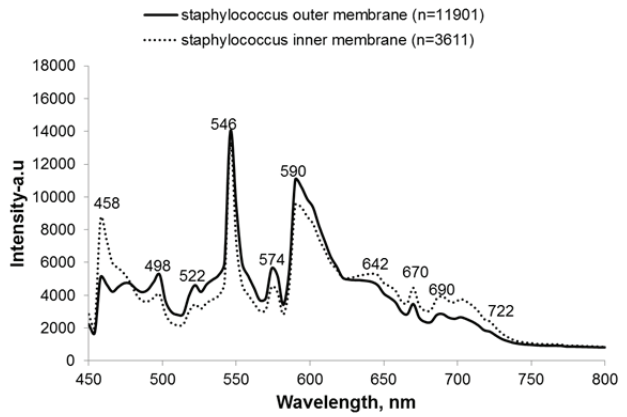

Figure 9. Comparison of spectral signatures from inner and outer membranes of gram-positive (*Staphylococcus aureus*) bacterial cells.

690 nm. However, the SD of each spectrum varied with the wavelength.

Table 2 summarizes the mean and SD values of scattering intensity and the percent variation at the peak wavelengths for *Staphylococcus* bacterial cells. In contrast with the gram-negative bacteria, higher spectral variations were observed for both the inner and outer membranes of the gram-positive *Staphylococcus* species in this study. Based on the spectral data for *Staphylococcus aureus*, higher

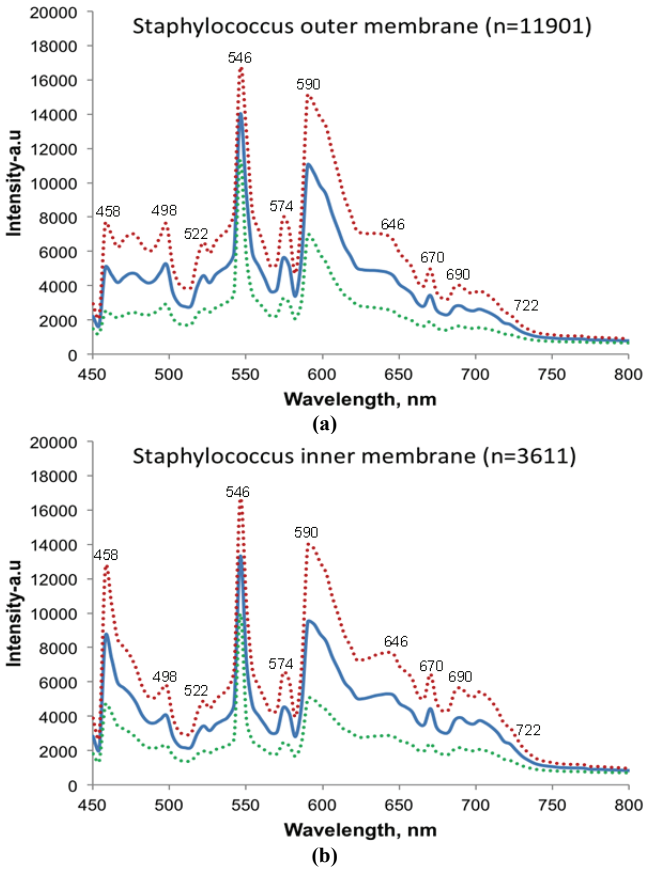

Figure 10. Mean and standard deviation of spectra from (a) outer and (b) inner membranes of gram-positive (*Staphylococcus aureus*) bacterial cells (solid line is mean scattering intensity, and dotted lines are standard deviation of intensity at observed spectral bands).

Table 2. Mean and standard deviation with corresponding wavelength of scattering intensity from *Staphylococcus aureus* as measured by the hyperspectral microscope imaging system.

Staphylococcus aureus	Wavelength (nm)	Mean	SD	Variation (%)
Inner membrane (n = 3,611)	458	8646	3970	46
	498	4056	1748	43
	522	3448	1471	43
	546	13323	3351	25
	574	4519	2054	45
	590	9509	4479	47
	646	5235	2409	46
	670	4456	2034	46
	690	3929	1757	45
	722	2400	967	40
	Average variation = 42.6%			
Outer membrane (n = 11,901)	458	5097	2569	50
	498	5272	2334	44
	522	4618	1942	42
	546	14012	2666	19
	574	5640	2361	42
	590	11051	4077	37
	646	4609	2070	45
	670	3471	1532	44
	690	2851	1178	41
	722	1779	591	33
	Average variation = 39.7%			

spectral variation (42.6%) was observed for the inner membrane than for the outer membrane (39.7%). In addition, the spectral variation of both the inner and outer membranes of *Staphylococcus* was much lower at 546 nm (25% inner and 19% outer), which was the strongest emission band for the metal-halide lighting source used in this experiment. The highest variation (47%) for the inner membrane was observed at 590 nm, followed by 46% at 458, 646, and 670 nm. However, the highest variation (50%) for the outer membrane was observed at 458 nm, followed by 45% at 646 nm. For the gram-positive bacteria, the spectral variation at the other scattering peaks was between 40% and 45% for the inner membrane, while the range of spectral variation for the outer membrane was wider (between 33% and 44%). This higher scattering variability for the outer membrane could be more sensitive to darkfield illumination than the inner membrane of the gram-positive bacteria.

HYPERSPECTRAL IMAGE OF *STAPHYLOCOCCUS SIMULANS* WITH ROI

For data collection from the five *Salmonella* serotypes and five *Staphylococcus* species described in the sample preparation section, an auto-threshold method was used. Figure 11 shows a hyperspectral microscope image and corresponding ROI for data collection from *Staphylococcus simulans* with the auto-threshold method. Image data were collected from *Salmonella* at 546 nm using minimum threshold values of 4,000 for Typhimurium, 5,000 for Heidelberg and Infantis, and 6,000 for Enteritidis and Kentucky. The maximum value was fixed at 15,000 for quality image data from the gram-negative bacteria. A spectral image at 550 nm was chosen as a template for *Staphylococcus*. In this case, the minimum threshold values were 5,000 for *haemolyticus*, 6,000 for *aureus*, 7,000 for *hyicus*, 8,000 for *sciuri*, and 9,000 for *simulans*. The maximum threshold was selected as 20,000 for all species. With the selected

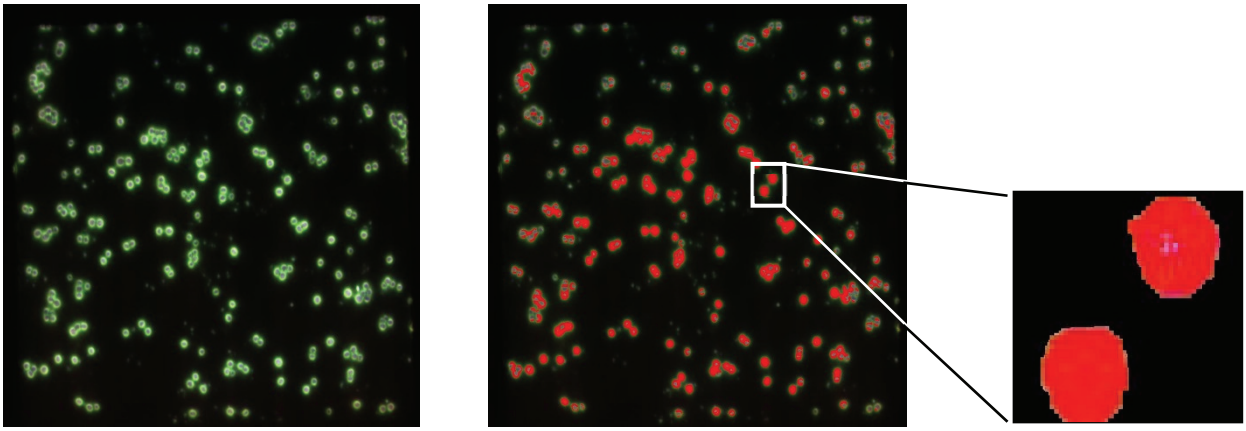

(a) (b)

Figure 11. (a) Hyperspectral microscope image and (b) corresponding region-of-interest (ROI) for analysis of data collected from *Staphylococcus simulans* with auto-threshold method (minimum = 9,000 and maximum = 20,000).

threshold values, a total of 483,547 pixels from *Salmonella* and 219,027 pixels from *Staphylococcus* were collected for further data analysis. For efficient data acquisition from bacterial cells, additional research needs to be conducted to select the optimum threshold values from various bacteria samples.

Spectral Signatures of Gram-Negative and Gram-Positive Bacteria

Figure 12 shows a comparison of the spectral signatures from the five gram-negative *Salmonella* serotypes, including Enteritidis (n = 81,315), Typhimurium (n = 67,078), Kentucky (n = 124,116), Heidelberg (n = 139,539), and Infantis (n = 71,499), and the five gram-positive *Staphylococcus* species, including *simulans* (n = 38,377), *sciuri* (n = 33,860), *hyicus* (n = 81,316), *haemolyticus* (n = 28,251), and *aureus* (n = 37,223). Overall, the scattering intensity from the gram-positive *Staphylococcus* species was higher than that of the gram-negative *Salmonella* serotypes at all wavelengths of 458, 498, 522, 546, 574, 590, 642, 670, and 690 nm.

As seen in figure 13, the scattering intensity from the inner cell membrane of *Staphylococcus* was higher than any other scattering intensity at 458, 642, 670, and 690 nm. However, the highest scattering intensity peaks were observed at 496, 546, 574, and 590 nm for the outer membrane of *Staphylococcus*. Figure 14 confirms that the scattering intensity of gram-negative bacteria (*Salmonella*) was lower than that of gram-positive bacteria (*Staphylococcus*) at all peak wavelengths compared.

Comparison of Spectral Signatures of *Salmonella* and *Staphylococcus*

The mean, SD, and percent variation values of peak scattering intensity with corresponding wavelengths are summarized in tables 3 and 4 for *Salmonella* and *Staphylococcus*, respectively. The variation in scattering intensity for *Salmonella* (31.2%) was lower than that of *Staphylococcus* (42.7%). The intensity variation for *Salmonella* in the NIR region (722 nm) was much lower than at visible wavelengths. The highest variation (37%) was observed at 594 nm, followed by 498 and 522 nm (both 34%). The lowest variation of scattering intensity for *Staphylococcus*

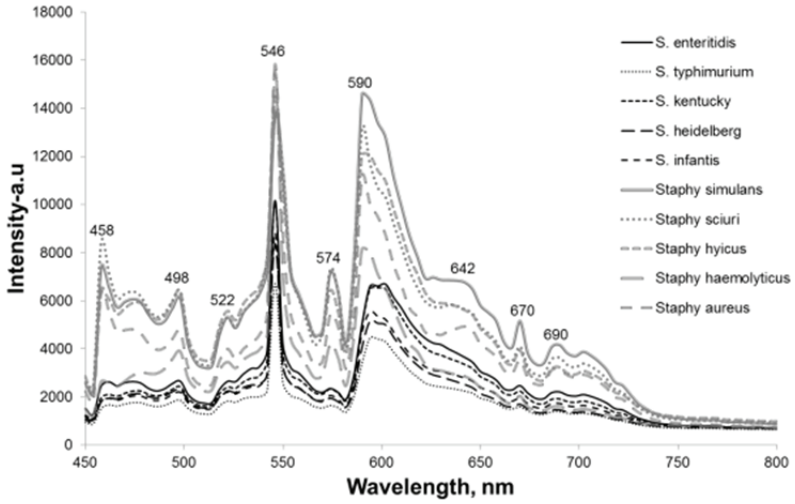

Figure 12. Comparison of spectral signatures from five gram-negative bacteria (*Salmonella* serotypes: Enteritidis, Typhimurium, Kentucky, Heidelberg, and Infantis) and five gram-positive bacteria (*Staphylococcus* species: *simulans*, *sciuri*, *hyicus*, *haemolyticus*, and *aureus*).

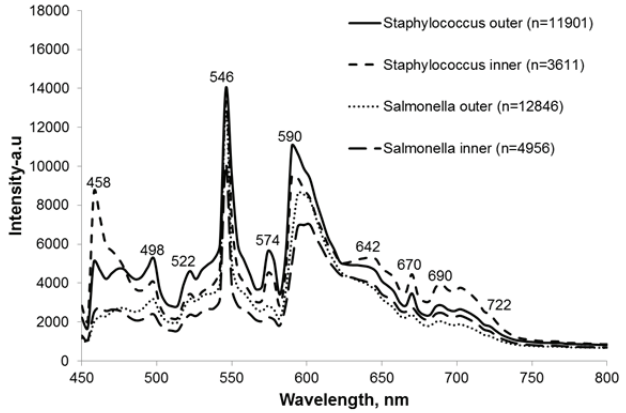

Figure 13. Comparison of spectra between the inner and outer cell membranes of *Staphylococcus* and *Salmonella* bacteria.

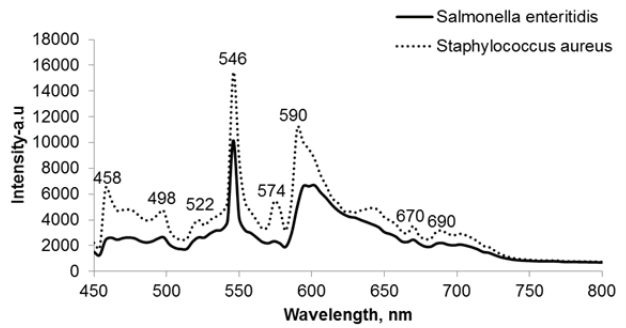

Figure 14. Comparison of spectra between gram-negative (*Salmonella*) and gram-positive (*Staphylococcus*) bacteria.

Table 3. Mean and standard deviation with corresponding wavelength of scattering intensity from gram-negative bacteria (*Salmonella*) as measured by the hyperspectral microscope imaging system.

Salmonella	Wavelength (nm)	Mean	SD	Variation (%)
Inner and outer membranes (n = 17,802)	462	2420	740	31
	498	2953	1008	34
	522	2962	1006	34
	546	12140	3672	30
	574	2666	888	33
	594	8146	3002	37
	642	3893	1255	32
	670	2482	725	29
	690	2157	624	29
	722	1347	310	23
	Average variation = 31.2%			

Table 4. Mean and standard deviation with corresponding wavelength of scattering intensity from gram-positive bacteria (*Staphylococcus*) as measured by the hyperspectral microscope imaging system.

Staphylococcus	Wavelength (nm)	Mean	SD	Variation (%)
Inner and outer membranes (n = 15,512)	458	5923	3314	56
	498	4989	2271	46
	522	4346	1908	44
	546	13851	2855	21
	574	5379	2342	44
	590	10692	4224	40
	646	4755	2170	46
	670	3700	1714	46
	690	3102	1411	45
	722	1923	744	39
	Average variation = 42.7%			

was observed at 546 nm, which was the highest emission intensity of the metal-halide lighting source, and the highest intensity variation (56%) was observed at 458 nm, followed by the second highest (46%) at 498, 646, and 670 nm.

Classification Accuracy for Gram-Negative and Gram-Positive Bacteria

Table 5 shows the classification accuracy, as a confusion matrix, of the five methods used to classify the gram-negative (*Salmonella*) and gram-positive (*Staphylococcus*) bacteria. All five methods (kNN, LDA, QDA, SVM, and MD) had high accuracy (>99%) in classifying *Salmonella* and *Staphylococcus*. These classification models also had very low (≤0.45%) false errors. Specifically, *Salmonella* bacteria were perfectly classified from *Staphylococcus* by LDA and MD, while *Staphylococcus* bacteria were identified with 100% accuracy by QDA and SVM.

Comparison of Classification Accuracy with Different Methods

Table 6 shows a comparison of the classification accuracy in identifying gram-positive and gram-negative foodborne pathogens with the five classification algorithms. The overall best classification was obtained with SVM (99.99%), followed by MD (99.98%), kNN (99.98%), LDA (99.98%), and QDA (99.75%). The classification models have kappa coefficients of 0.9998, 0.9995, 0.9995, 0.9995, and 0.9937, respectively, which indicates that all models have very good agreement with high reliability. Thus, all models tested for gram-negative and gram-positive foodborne bacteria demonstrated mean classification accuracy of 99.8% with a mean kappa coefficient of 0.9984.

Table 5. Confusion matrix for classification accuracy of gram-negative (*Salmonella*) and gram-positive (*Staphylococcus*) bacteria by five different methods (*N* = 703,000 total data, *N* = 23,000 for calibration, and *N* = 680,000 for validation).

Method[a]	Actual	Prediction (%) *Salmonella*	Prediction (%) *Staphylococcus*
kNN	*Salmonella*	99.98	0.02
	Staphylococcus	0.02	99.98
LDA	*Salmonella*	100.00	0.04
	Staphylococcus	0.00	99.96
QDA	*Salmonella*	99.55	0.00
	Staphylococcus	0.45	100.00
SVM	*Salmonella*	99.99	0.00
	Staphylococcus	0.01	100.00
MD	*Salmonella*	100.00	0.02
	Staphylococcus	0.00	99.98

[a] kNN = *k*-nearest neighbor, LDA = linear discriminant analysis, QDA = quadratic discriminant analysis, SVM = support vector machine, and MD = Mahalanobis distance.

Table 6. Classification accuracy to detect gram-positive and gram-negative foodborne pathogens with five classification algorithms.[a]

	MD	kNN	LDA	QDA	SVM	Mean
Accuracy	99.98%	99.98%	99.98%	99.75%	99.99%	99.8%
Kappa	0.9995	0.9995	0.9995	0.9937	0.9998	0.9984

[a] The total number of data was 703,000, of which 23,000 (30%) were used for calibration and 680,000 (70%) were used for validation.

CONCLUSIONS

A method of acousto-optic tunable filter (AOTF)-based hyperspectral microscope imaging has potential for rapid identification of foodborne pathogenic bacteria from microcolonies (less than 1 min for scanning each sample on a glass slide) with a cell level. In this study, we successfully developed a method to acquire quality hyperspectral microscopic images from various gram-negative and gram-positive bacteria live cells. Among the contiguous spectral images in the visible/NIR region between 450 and 800 nm, the scattering intensity was distinct at mostly visible wavelengths. Specifically, the scattering peak intensity was distinct at 458, 498, 522, 546, 574, 590, 646, 670, and 690 nm for *Staphylococcus*. Similarly, distinct peak spectra were observed at 462,498, 522, 546, 574, 598, 642, 670, and 690 nm for *Salmonella*. For both cases, the scattering intensity of the outer cell membrane was higher than that of the inner membrane except at 546 nm, which was possibly caused by excitation of the metal-halide lighting source. The scattering intensity from a single cell varied with the wavelength as well as the type of bacteria. The overall variability of intensity was 31.2% for the gram-negative bacteria (*Salmonella*) and 42.7% for the gram-positive bacteria (*Staphylococcus*). Using the scattering intensity data from the bacterial cells, a classification accuracy of 99.99% and kappa coefficient of 0.9998 were obtained with support vector machine (SVM). However, the classification models need to be validated with bacterial cultures from more food matrices. Further research is also needed to validate the method with positively identified colonies using confirmatory testing, such as latex agglutination or polymerase chain reaction (PCR) tests.

ACKNOWLEDGEMENTS

The authors would like to thank Dr. Sun Choi, Dr. Nasreen Bano, Jerrie Barnett, and Matthew Eady of the USDA-ARS Quality and Safety Assessment Research Unit in Athens, Georgia, for their assistant for this research. This project is partially supported by the National Institute for Hometown Security (KCU No. 01-09-UK).

REFERENCES

CDC. (2011). FoodNet surveillance report for 2010 (Final report). Atlanta, Ga.: Centers for Disease Control and Prevention, Foodborne diseases active surveillance network (FoodNet). Retrieved from www.cdc.gov/foodnet/PDFs/2010_annual_report_508c.pdf.

CDC. (2012). Foodborne outbreak online database. Atlanta, Ga.: Centers for Disease Control and Prevention, National Center for Emerging and Zoonotic Infectious Diseases.

Correa, A. A., Toso, J., Albarnaz, J. D., Simoes, C. M. O., & Barardi, C. R. M. (2006). Detection of *Salmonella* Typhimurium in oysters by PCR and molecular hybridization. *J. Food Qual., 29*(5), 458-469. http://dx.doi.org/10.1111/j.1745-4557.2006.00086.x.

De Maesschalck, R., Jouan-Rimbaud, D., & Massart, D. L. (2000). The Mahalanobis distance. *Chemometrics Intel. Lab. Syst., 50*(1), 1-18. http://dx.doi.org/10.1016/S0169-7439(99)00047-7.

Dixon, S. J., & Brereton, R. G. (2009). Comparison of performance of five common classifiers represented as boundary methods: Euclidean distance to centroids, linear discriminant analysis, quadratic discriminant analysis, learning vector quantization, and support vector machines, as dependent on data structure. *Chemometrics Intel. Lab. Syst., 95*(1), 1-17. http://dx.doi.org/10.1016/j.chemolab.2008.07.010.

Furey, T. S., Cristianin, N., Duffy, N., Bednarski, D. W., Schummer, M., & Haussler, D. (2000). Support vector machine classification and validation of cancer tissue samples using microarray expression data. *Bioinfomatics, 16*(10), 906-914. http://dx.doi.org/10.1093/bioinformatics/16.10.906.

ISO. (2002). ISO 6579: Microbiology of food and animal feeding stuffs: Horizontal method for the detection of *Salmonella* spp. Geneva, Switzerland: International Standards Organization.

MMWR. (2013). Outbreak of *Staphylococcal* food poisoning from a military unit lunch party: United States, July 2012. *Morbidity Mortality Weekly Report, 62*(50), 1026-1028.

Munson, T. E., Schrade, J. P., Bisciello Jr, N. B., Fantasia, L. D., Hartung, W. H., & O'Connor, J. J. (1976). Evaluation of an automated fluorescent antibody procedure for detection of *Salmonella* in foods and feeds. *Appl. Environ. Microbiol., 31*(4), 514-521.

Park, B., Yoon, S. C., Lawrence, K. C., & Windham, W. R. (2007). Fisher linear discriminant analysis for improving fecal detection accuracy with hyperspectral images. *Trans. ASABE, 50*(6), 2275-2283. http://dx.doi.org/10.13031/2013.24080.

Park, B., Yoon, S. C., Lee, S., Sundaram, J., Windham, W. R., Hinton Jr., A., & Lawrence, K. C. (2012 a). Acousto-optic tunable filter hyperspectral microscope imaging for identifying foodborne pathogens. *Trans. ASABE, 55*(5), 1997-2006. http://dx.doi.org/10.13031/2013.42345.

Park, B., Windham, W.R., Ladely, A. R., Gurram, P., Kwon, H., Yoon, S.C., Lawrence, K. C., Narrange, N., & Cray, W. C. (2012b). Classification of Shiga toxin-producing *Escherichia coli* (STEC) serotypes with hyperspectral microscope imagery. *Proc. SPIE 8369*, doi: 10.1117/12.919695.

Scharff, R. (2012). Economic burden from health losses due to foodborne illness in the United States. *J. Food Prot., 75*(1), 123-131. http://dx.doi.org/10.4315/0362-028X.JFP-11-058.

Tian, H., Miyamoto, T., Okabe, T., Kuramitsu, Y., Honjoh, K. I., & Hatano, S. (1996). Rapid detection of *Salmonella* spp. in foods by combination of a new selective enrichment and a sandwich ELISA using two monoclonal antibodies against dulcitol 11-phosphate dehydrogenase. *J. Food Prot., 59*(11), 1158-1163.

USDA-FSIS. (2014). *Microbiology Laboratory Guidebook*. Washington, D.C.: USDA Food Safety and Inspection Service.

Vandeginste, B. M. G., Massart, D. L., Buydens, L. M. C., De Jong, S., Lewi, P. J., & Smeyers-Verbeke, J. (1998). *Handbook of Chemometrics and Qualimetrics: Part B*. Amsterdam, The Netherlands: Elsevier.

Velusamy, V., Arshak, K., Korostynska, O., Oliwa, K., & Adley, C. (2010). An overview of foodborne pathogen detection: In the perspective of biosensors. *Biotech. Adv., 28*(2), 232-254. http://dx.doi.org/10.1016/j.biotechadv.2009.12.004.

Wang, W., Li, C., Tollner, E. W., Gitaitis, R., & Rains, G. (2012). A liquid crystal tunable filter based shortwave infrared spectral imaging system: Design and integration. *Comp. Electron. Agric., 80*, 126-134. http://dx.doi.org/10.1016/j.compag.2011.07.012.

Windham, W. R., Yoon, S. C., Ladely, S. R., Heitschmidt, G. W., Lawrence, K. C., Park, B., Narang, N., & Cray, W. C. (2012). The effect of regions of interest and spectral pre-processing on the detection of non-O157 Shiga-toxin producing *Escherichia coli* serogroups on agar media by hyperspectral imaging. *J. Near-Infrared Spectrosc., 20*(5), 547-558. http://dx.doi.org/10.1255/jnirs.1004.

Wu, W., Mallet, Y., Walczak, B., Penninckx, W., Massart, D. L., Heurding, S., & Erini, F. (1996). Comparison of regularized

discriminant analysis, linear discriminant analysis, and quadratic discriminant analysis, applied to NIR data. *Analytica Chimica Acta, 329*(3), 257-265. http://dx.doi.org/10.1016/0003-2670(96)00142-0.

Yoon, S. C., Lawrence, K. C., Siragusa, G., Line, J., Park, B., & Feldner, P. (2009). Hyperspectral reflectance 513 imaging for detecting a foodborne pathogen: *Campylobacte*r. *Trans. ASABE, 52*(2), 651-662.http://dx.doi.org/10.13031/2013.26814.

Yoon, S. C., Windham, W. R., Ladely, S. R., Heitschmidt, G. W., Lawrence, K. C., Park, B., Narang, N., & Cray, W. C. (2013). Hyperspectral imaging for differentiating colonies of non-O157 Shiga-toxin producing *Escherichia coli* (STEC) serogroups on spread plates of pure cultures. *J. Near-Infrared Spectrosc., 21*(2), 81-95. http://dx.doi.org/10.1255/jnirs.1043.